Deformation analysis on F138 austenitic stainless steel: ECAE and rolling

2014 IOP Conf. Ser.: Mater. Sci. Eng. 63 012057

(http://iopscience.iop.org/1757-899X/63/1/012057)

IOP Conf. Series: Materials Science and Engineering **63** (2014) 012057 doi:10.1088/1757-899X/63/1/012057

Deformation analysis on F138 austenitic stainless steel: ECAE and rolling

N S De Vincentis[1], M C Avalos[1], A M Kliauga[2], V L Sordi[2], N Schell[3], H-G Brokmeier[3], R E Bolmaro[1]

[1] Instituto de Física Rosario - IFIR, National University of Rosario, Rosario Argentina.
[2] Materials Engineering Department, São Carlos Federal University, São Carlos, Brazil.
[3] Institut für Werkstoffkunde und Werkstofftechnik, TU Clausthal, Agricolastr. 6, 38678 Clausthal-Zellerfeld-Helmholtz-Zentrum Geesthacht, GEMS Outstation, Notkestr. 85, 22607 Hamburg, Germany.
E-mail: kliauga@ufscar.br

Abstract. Twinning is an alternative mechanism to achieve ultra-fine grain structures through severe plastic deformation. The properties induced in a plastically deformed material are highly dependent on the degree of deformation, accumulated deformation energy and details on grain sizes and microstructure, which are on the scale of some tens of nanometers; therefore it is very important to understand misorientation distributions and dislocation arrays developed in the samples. In this work an F138 austenitic stainless steel was solution heat treated, deformed by Equal Channel Angular Extrusion (ECAE) at room temperature up to four passes, and rolled up to 70% thickness reduction at room temperature. The microstructure evolution was analyzed by x-ray diffraction and domain sizes calculated by Convolutional Multiple Whole Profile (CMWP) model, the misorientation boundaries were measured by electron backscattered diffraction (EBSD), and transmission electron microscopy. Mechanical behavior was tested by tensile tests.

Keywords: equal channel angular pressing, austenitic stainless steel, x-ray analysis, domain size

1. Introduction

Equal channel angular extrusion (ECAE) is a technique whose main advantage is the production of fine-grained materials with outstanding tensile strengths. The technique uses two square or circular die channels intersecting at a given preselected angle Φ. At the intersection the material undergoes simple shear deformation to an extent that depends on the intersection angle. Since the sample section is kept constant the process can be repeated as intended and therefore used to achieve severe plastic deformation (SPD). [1-4].

During SPD of medium to high stacking fault energy (SFE) metals (e.g. Cu, Ni and Al) the microstructure evolves through the formation of dislocation cells [5]. In contrast, in low SFE metals (such as austenitic stainless steel, brass, Al–Mg alloys, and Cu–Al alloys) deformation leads to twins and second-generation microbands rather than dislocation cells [6].

For coarse grain materials, S Asgari et al. [7] and El-Danaf et al. [8] reported that low SFE fcc metals exhibit four distinct strain-hardening stages in simple compression tests. They correlated different strain hardening rates with the activation of different deformation mechanisms:

- stage A similar to deformation stage II correlated with multiple dislocation slip;

- stage B correlated with the initiation of twinning deformation, and the critical dislocation density enough to activate that mechanism;
- stage C correlated with a decreasing rate of primary twinning and
- stage D reflects the stress concentration for a new twin to shear an existing twin with the presence of extensive twin intersections.

They also observed that the twin initiation was shifted to higher stress values when the grain size decreased, and was suppressed when grain size was reduced from 40 to 9 μm. Similar results were obtained by Ueji et al. [9] and Gutierrez- Urrutia et al [10] in TWIP steels. They observed that twinning was more difficult and the influence of the resolved shear stress increased when grain size was reduced to 3 – 2 μm.

Conversely, for ultrafine grain fcc metals it may be easier to deform by twinning with decreasing grain size, reaching a maximum twinning probability and then becoming more difficult again when the grain size decreases further, i.e. an inverse grain-size effect on twinning [11]. Recent TEM observations in fcc metals, such as Al [*12*.], Cu [*13*.], Ni [*14*], etc., showed that in nano-crystalline or ultra-fine grained boundaries, deformation twins and stacking faults, indicating the presence of partial dislocation mediated processes, might be considered as contributing deformation mechanisms.

Deformation twinning transforms the homogeneously deformed fcc structures into fine lamellar structures, which will be further divided by the twin-matrix layers and intersections of other twins. The grain rotation and/or grain boundary migration result in a large number of misfit dislocations or partial dislocations at grain boundaries, which mediates nucleation of deformation twins in the fine grain structure [15]. Nano-twinning was also shown to be a critic factor in the development of micro-structure enabling a favorable combination of strength and ductility for copper processed at low-temperature through ECAE followed by cryo-drawing and cryo-rolling [16.] and for the low SFE SUS316L austenitic stainless steel [17,18.].

The properties induced in a plastically deformed material, either by ECAE or rolling, are highly dependent on the degree of deformation, accumulated deformation energy and details on grain sizes (in the tens of nanometers) and microstructure. The presence of defects in the microstructure, such as dislocation arrays, stacking faults, etc. determines a distortion in the crystallographic structure of the material, restricting the motion of other defects; therefore it is very important to understand the development of misorientation distributions and dislocation arrays [19,20].

The most used technique for local analysis is transmission electron microscopy (TEM), which allows seeing in detail the dislocation structure and arrays, grain boundaries, and crystallographic structures almost point by point because of the small volume interaction. This advantage, due to the high resolution of the technique, turns into a drawback when a statistical analysis is needed because of the low amount of information provided.

To overcome this difficulty, since the ’50s several methods have been developed for characterizing the microstructure of bulk materials by x-ray diffraction experiments, which are based on the fact that the defects induced in a material through deformation have a direct impact on the characteristics of the diffraction profile [21]. In such way, an analysis of the broadening of the diffraction peaks would allow to determine the diffraction domain sizes and the dislocation and stacking fault densities. One of the first micromechanical models created to assess these variables was the Williamson-Hall (W-H) method [21], later on modified by Ungár [19,22] and Warren [23,24**]** (MW-H). Both methods allow the analysis of large volumes of the material, several hundreds of microns in depth and mm size in surface lengths. The capability for detecting misorientations between diffraction domains depends on the resolution of the instrument, which is determined mostly by the angular dispersion of the incident radiation (machine peak broadening). For a conventional diffractometer this

dispersion is on the tenths of a degree, while for synchrotron light facilities the dispersion is less than that, improving the resolution accordingly.
More recently the technique of Orientation Imaging Microscopy (OIM) or Electron Back Scatter Diffraction (EBSD) came on action. It can automatically obtain and analyze Kikuchi patterns and determine crystalline orientations in areas of some μm^2 in size, improving the statistics [25, 26]. This method can perceive misorientations greater than 0.5 degrees, and the obtained information can be viewed in orientation maps, charts, pole figures, etc. One of the purposes of this research is to compare and unite all the results, obtained using the mentioned techniques, to evaluate the microstructural changes caused by deformation in an ECAE deformed F138 austenitic stainless steel.

2. Experimental Procedure

A commercial F138 alloy, with the composition, in wt%, 0.015 C, 0.079 N, 17.33 Cr, 14.31 Ni, 1.79 Mn, 2.79 Mo, 0.3 Si, 0.002 S, 0.0022 P, was solution heat treated at 1100°C for 1 hour and quenched. ECAE deformation was performed in a 120° die with the angle subtending the outer curvature radius equal to 20° and circular cross section channels with a diameter of 10 mm. The accumulated strain was estimated by the equation:

$$\varepsilon_{ECAP} = \frac{N}{\sqrt{3}}.2\left(\cot\left(\frac{\phi}{2}+\frac{\psi}{2}\right)+\psi\,\mathrm{cosec}\left(\frac{\phi}{2}+\frac{\psi}{2}\right)\right) \qquad \text{(Eq. 1)}$$

where φ and ψ are the corner angle and the die angle, respectively, and N is the number of passes [27]. For the used configuration the equivalent strain per pass is about 0.67. The material was pressed till four passes without rotation in the extrusion axis (route A), yielding equivalent deformations of 0.67, 1.34 and 2.68 respectively.
One set of samples was rolled till 70% thickness reduction with 10% reduction per pass, yielding a total equivalent deformation of 1.38.
Tensile tests were performed in an INSTRON universal testing machine, in sub-size samples with a gauge length of 7 mm and 3 mm x 2 mm cross section area. The elongation was monitored by an optical extensometer. The tests were performed at room temperature and at a nominal strain rate of $1 \times 10^{-3}\ s^{-1}$.
Optical and scanning electron microscopy observation of the microstructure was performed in the plane perpendicular to the transverse direction (TD). The samples were prepared by conventional polishing techniques followed by a final polishing in 0.05 μm acid colloidal silica. EBSD analysis was performed in a FEI Quanta 200 scanning electron microscope (SEM) equipped with automatic OIM and TSL-EDAX software. The ECAE processed samples are identified by the letter X, preceded by a number indicating the pass number: 1X, 2X and 4X. The OIM scans of the rolled 1X and 2X samples were done with a step size of 70 nm, the 4X sample was done with a step size of 40 nm. To get similar coverage for 70 nm and 40 nm step sizes, Kernel Average Misorientation (KAM) were calculated with 4 or 7 neighbours and a maximum misorientation of 3° was chosen as appropriate for current domain sizes.
TEM samples were prepared by electrolytic polishing (10% $HClO_4$ in alcohol, 30V 0°C) and observed in a CM120 FEI microscope.
The diffraction experiments were conducted using a SIEMENS D5000 diffractometer using CuKα radiation and on GEMS outstation, Petra III, DESY, Hamburg synchrotron line. Synchrotron data was collected in transmission by a Mar345 image plate, composed of 3450 x 3450 square pixels (100 μm x 100 μm) and later on reduced by Fit2D software to calculate difractograms on different sample directions. On those diffractograms, peak broadening was analyzed by the Williamson-Hall (W-H) method [21], modified by Ungár [22, 24] and Warren [23] (MW-H) by using the following equation:

$$\frac{Breathcos\theta}{\lambda} - \beta W_g = \frac{1}{d} + \left(\frac{\pi M^2 b^2}{2}\right)\rho^{1/2} K^2 C \qquad \text{(Eq.2)}$$

where d is the diffraction domain size, λ is the wavelength of the radiation, β is the stacking fault density, Wg are the Warren constants related to the stacking faults, ρ is the dislocation density, b is the Burgers vector, M is a constant related to the cut-off radius of dislocations (which is smaller for more compact arrays), C are the average contrast factors of dislocations and K=2Sin(θ)/λ. Another way of analyzing peak breadth is to use the Convolutional Multiple Whole Profile model (CMWP) [23], which uses a fitting algorithm that compares the real diffraction pattern with a mathematical function that is created by the user, pretty much like the ones used for Rietveld analysis but depending mainly on the microstructural features. In this work both methods were compared.

3. Results and Discussion

The austenitic microstructure appears to be reasonably stable under the present pressing conditions. No evidence of martensitic transformation during ECAE has been found by x – ray diffraction, as shown in Figure 1.

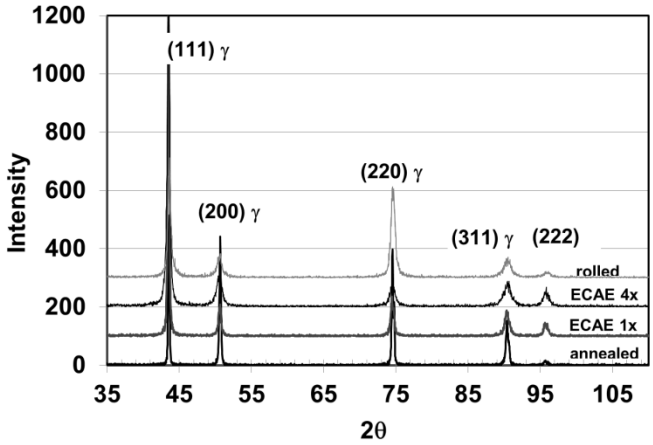

Figure 1: X –ray diffraction analysis (CuKα) of the F138 deformed by ECAE and rolled 70%.

The undeformed sample showed coarse grains containing recrystallization twins. Figure 2 shows the Image Quality (IQ) maps of samples as annealed, 1X, 2X, 4X and rolled. The dark lines mark borders of misorientation, that is, sub-grains and grains, twin boundaries, zones of high density of dislocation cells and shear bands. Deformation twins cannot be distinguished from other boundaries because the actual distance between the two boundaries usually is of the order of 10 nm, hence smaller than the measuring step size, but they appear as straight lines crossing the entire grain (Figure 2b). After the second ECAE pass, the first twin boundaries are bent, secondary twinning, transverse to the primary twin boundaries, have been formed and there was an increase in accumulated deformation near to the initial grain boundaries (Figure 2c). The same features are seen in the rolled sample (Figure 2e). For the sample of four ECAE passes, the microstructure is subdivided by shear bands and dislocation cells (Figure 2d).

The volume fraction of twins in the first ECAE pass at room temperature was 60 ± 10 % measured from TEM images. Detailed features of the microstructure of sample 2X is shown

in Figure 3. The microstructure is composed of two fairly different types of structural units: a banded microstructure consisting of multiple mechanical twin bundles embedded into a severely deformed matrix. The original grains are subdivided into regions of same crystal orientation separated by high angle twin boundaries of stages A and B. These are further deformed, losing its twin character and form deformation bands in which dislocation cells and microtwin bundles will act in the formation of new sub-micron grains. High density dislocation configurations are seen in TEM images (Fig. 3b). These dislocations are supposed to be responsible for the high elastic strains accumulated in the lattice during ECAE.
After four passes the bulk of the sample was constituted of these fine bands with a mean width of 50 nm, as shown in Figures 4a and b. Nano twins further subdivide these regions (see Fig. 4b).
Table 1 shows the mechanical properties obtained from the tensile tests. Yield strength and ultimate tensile strength increased three times after four passes ECAE. Total elongation is reduced from 60% in the as-received state to approximately 36% after the first pass and to 26% after four passes. This reduction is significant, yet not to an extent that would undermine the ability of the material to resist plastic deformation. The uniform elongation stage is small, amounting to about 2.5–3% in all ECAE samples. A short uniform elongation stage could reasonably be expected from the limited work hardening rate which is commonly observed after SPD, in accordance with Considère's criterion for the loss of macroscopic stability and the onset of necking [28]. Similar results were obtained by Ueno et al. [18] for the SUS 316L austenitic stainless steel.

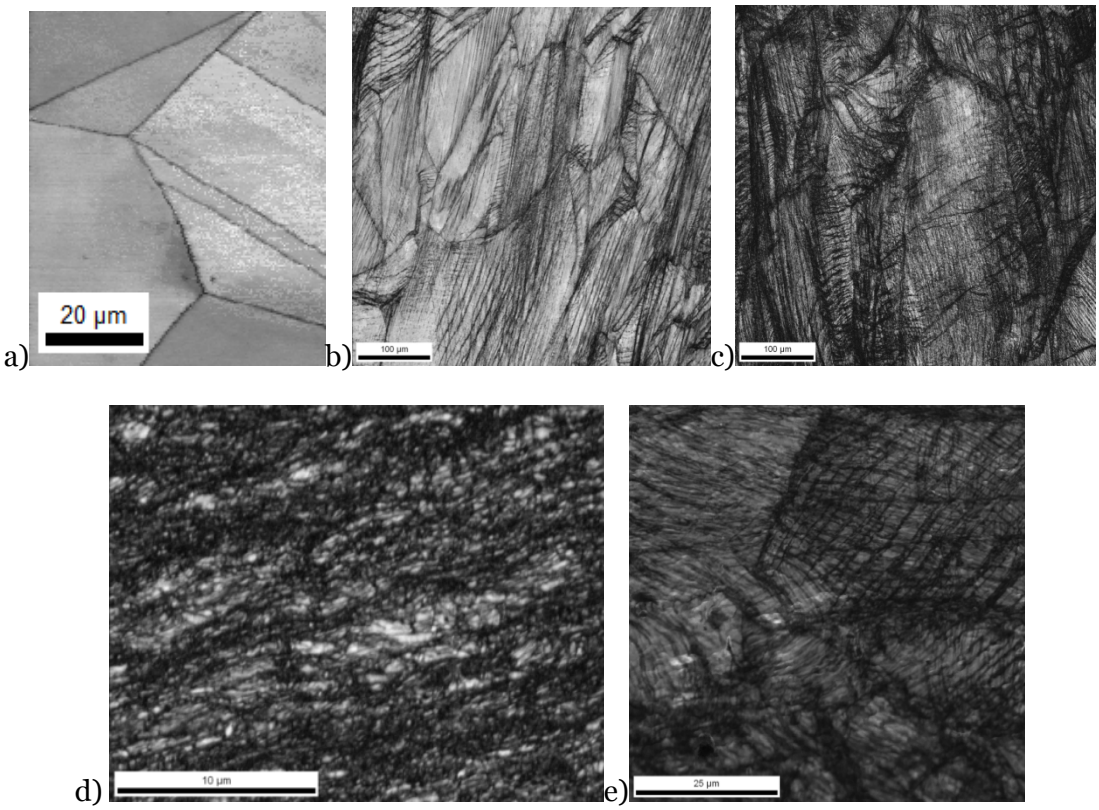

Figure 2. Image Quality maps obtained by EBSD: annealed sample (a); samples deformed by ECAE one (b), two (c) and four (d) passes; and the rolled sample (e).

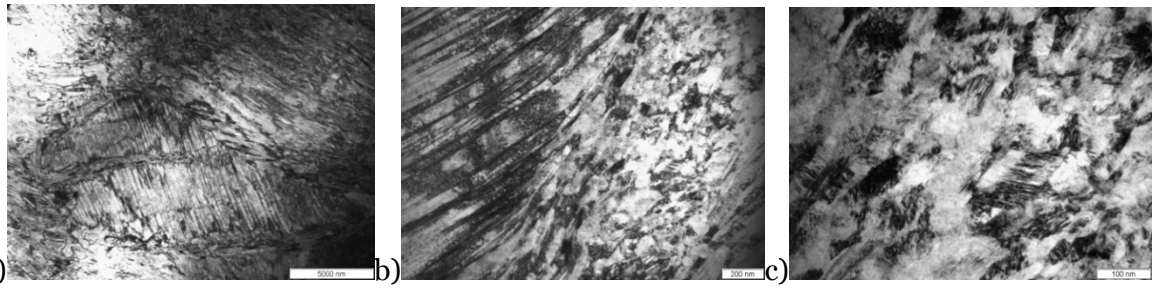

Figure 3. TEM images of the sample deformed by ECAE, two passes: a) general view; b) bended twin lamellae and shear band intersection ; c) nano twin bundles inside shear band.

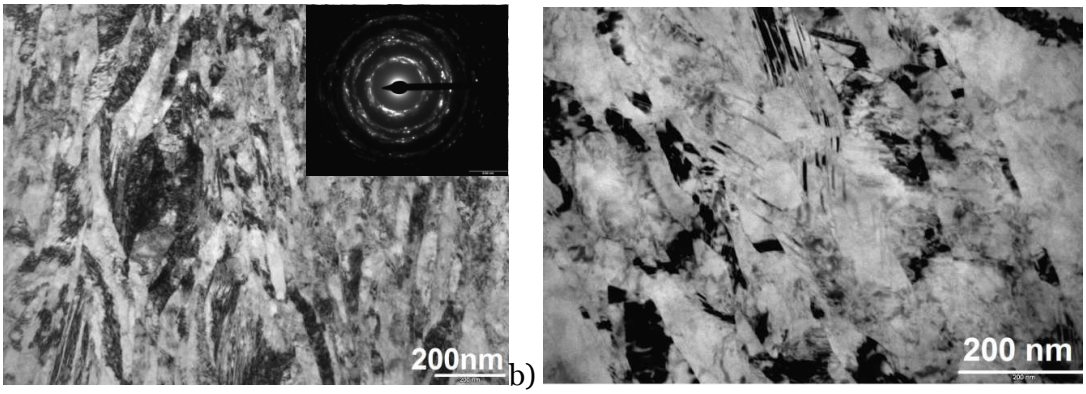

Figure 4: TEM images of the F138 steel deformed by four passes ECAE.

Table 1. Mechanical properties obtained by tensile and hardness tests: yield strength (σ_y), ultimate tensile strength (σ_u), total elongation (ε_t), uniform elongation (ε_u) and Vickers hardness (HV).

Sample	**σ_y (MPa)**	**σ_u (Mpa)**	**ε_t (%)**	**ε_u (%)**	**HV**
Initial	374	640	60	23	130
ECAE 1X	889	907	36	2.8	321
ECAE 2X	1055	1108	28	2.8	339
ECAE 4X	1140	1340	26	3,5	473
Rolled 70%	1100	1135	32	3,5	374

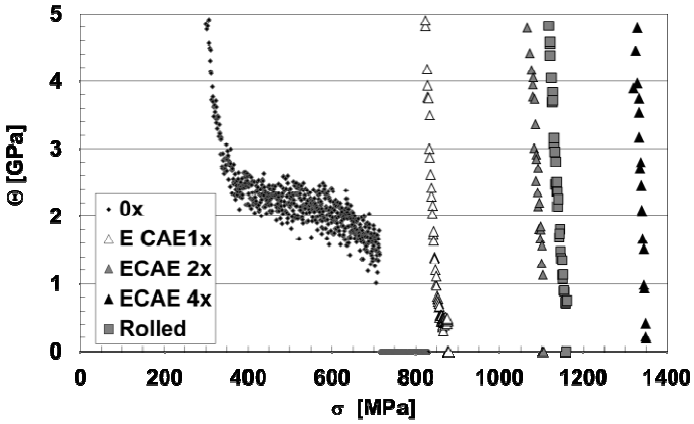

Figure 5. Strain hardening vs. true stress curves for the annealed (0x) and deformed samples ECAE one (1xRT) , two (2xRT) and four (4xRT) passes and rolled 70%.

At room temperature the original grains are subdivided into regions having the same crystal orientation, separated by high angle twin boundaries. The strain hardening curves obtained from the tensile tests can detect the first stage of twinning, which was shown to be active only for the annealed samples, as shown in Figure 5. Therefore, grain subdivision by twinning has already taken place at the beginning of the deformation; as secondary twinning demands higher stress levels, the deformation should proceed as a competition between dislocation glide and secondary twinning.

EBSD cannot detect absolutely every change in orientation due to twinning, because of lack of resolution at the level of a few nanometers, but can detect further deformation inside twined regions due to dislocation arrays formed by dislocation glide. Twinned regions are made evident by the highly distorted regions inside parallel planes that show the characteristic 60º change in orientation due to twining.

Regions limited by at least 3º misorientation were chosen as equivalent for the domain size and, inside them, regions delimited by lower angle boundaries were evidenced by calculating the Kernel Average Misorientations (KAM). Boundaries that were assumed to be sub-grains, dislocation boundaries (GND or IB) as well as twin boundaries are shown in Figures 6 a-b). According to the plots of Figure 6c), the KAM values increase with ECAE deformation, as well as the number of boundaries as shown in 6a)-b). The rolled sample has a theoretical equivalent deformation of the same order as the two passes ECAE sample, and yield stresses and ultimate strengths of the same order were measured for both. The KAM distributions for these two samples are also very similar but a higher amount of boundaries was detected for the rolled sample, as shown in Figure 6d).

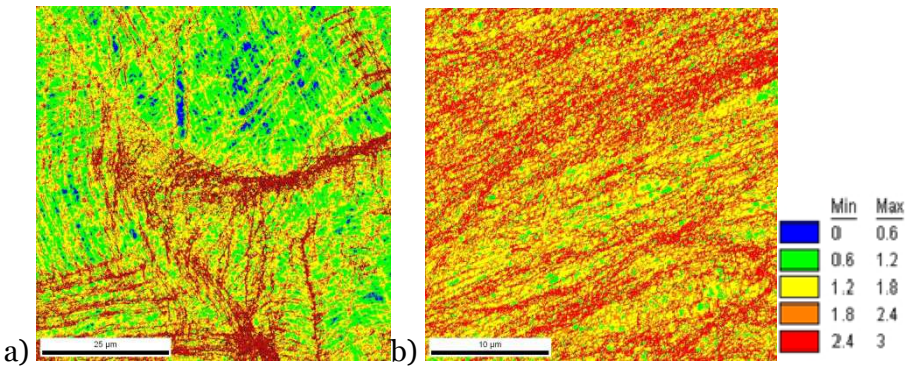

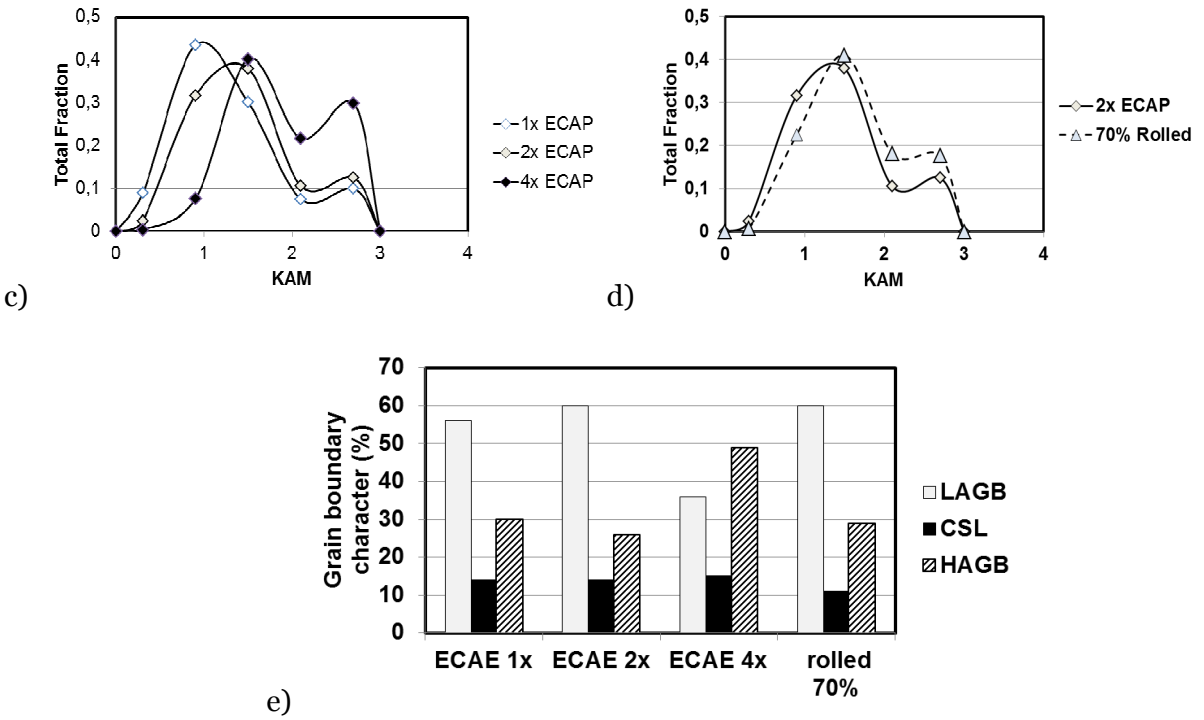

Figure 6. Kernel Average Misorientation (KAM) maps and charts obtained by EBSD. (a) ECAE 2 passes; (b) ECAE4 passes; (c) KAM distribution for the ECAE samples; (d) comparison between the KAM distribution of the ECAE 2 passes and 70% rolled sample; (e) fraction of measured low angle (LAGB), especial (CSL) and high angle (HAGB) grain boundaries .

The actual distribution of high angle grain boundaries (HAGB), boundaries of special character (coincident site lattice - CSL) and low angle grain boundaries (LAGB) is shown in Figure 6e. For the ECAE4x sample the amount of HAGB increased by 50%, showing that at this stage the process of formation of new sub-micron grains has begun.

The X-rays are more sensitive to changes in crystal orientations and residual strains due to dislocations that would not usually contribute to EBSD perceivable misorientations. The x-ray peak profiles were analyzed using both Williamsom-Hall (WH) and Convolutional Multiple Whole Profile (CMWP) model at the Normal (ND) and Transverse (TD) Directions to extrusion planes. Both methods give the same trends, but the WH tends to result in higher values for domain sizes, dislocation and stacking fault densities as shown in Figure 7. The measurements show larger differences between ND and TD for the ECAE samples than for the rolled sample because ECAE has higher deformation anisotropy along the sample thickness [4] and the transverse measurement represents a better mean across the bulk sample whereas the ND surface represents the measurement of a region subject to a higher amount of shear.

The domain size measurements are shown in Figure 7a. Dispersion, measured through the errors calculated by the standard deviation, is quite high for ECAE samples and lower for rolled sample, showing that domain sizes produced by ECAE are quite heterogeneous while rolling tends to produce a more homogeneous distributions. For the ECAE samples the domain sizes decreased between the first and second pass but increased after the fourth pass, while at the same time dislocation density has been reduced at the ND surface (see Figure 7b). This is an indication for the loss of cell interior dislocations to the walls where they get entrapped and further dynamically recover; this induce a gradual transformation of dislocation cell walls, or at least a large proportion of them, to high-angle grain boundaries

[30,31], leading to a continuous increase in the misorientation, as shown in figure 6. At the same time the amount of deformation twins increased (Figure 7c), indicating that secondary twinning is active and contributes to new grain subdivision.

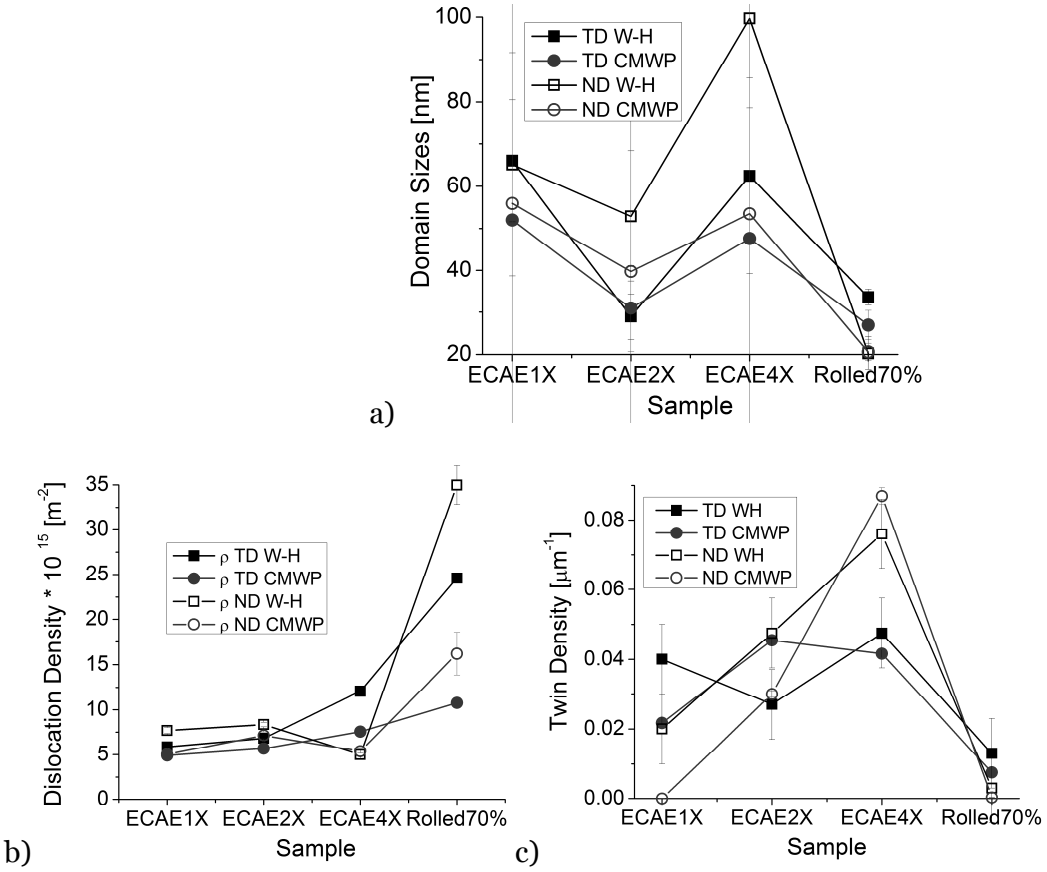

Figure 7. Results of peak breadth analysis: (a) domain size; (b) dislocation density, (c) twin density, on TD and ND directions as calculated by W-H and CMWP models.

When rolling is compared to ECAE, the rolling process can produce small diffraction domains, almost as much or smaller than ECAE processing, but with the particularity of still allowing a highly preferred orientation of the crystals, i.e. strong texture. It is necessary then to compare the effectiveness of both deformation techniques - ECAE and cold rolling - to obtain sub micrometer grain sizes and to study the particularities of the generated dislocation arrays. The amount of dislocation glide is much higher than that of stacking faults/twins for the rolled sample; this happens because deformation twinning is sensitive to deformation rate and temperature [6], and ECAE, because of geometrical reasons, proceeds much more localized and faster than rolling.

4. Summary and Conclusions

The nano/microstructural changes caused by deformation in an ECAE deformed F138 austenitic stainless steel was evaluated by TEM, EBSD and analysis of the peak broadening on synchrotron radiation diffraction data.

At room temperature original grains are subdivided into regions of same crystal orientation which take place at the beginning of the deformation; and while stress levels rise, secondary twinning is activated thus generating competition between dislocation glide and secondary twinning and contributing to fine grain formation.

After four passes ECAE a fine lamellar structure (50 nm wide) was produced. These lamellae are further subdivided by secondary twins. Both x-ray analysis and EBSD demonstrate that dynamic recrystallization has started with the increase of the fraction of HAGB, the increase of domain size and reduction of the dislocation density.
EBSD is a technique allowing the detection of deformation inside twined regions due to dislocation arrays formed by dislocation glide. Orientation changes very close to 60^{o} are a signature for detecting twining, although even at high resolution the profuse nano-structure generated by twining cannot quantitatively evaluated.
By energetic synchrotron X-rays not only changes in crystal orientations but also residual strains generated by dislocations and stacking faults, that would not usually be accurately perceivable by EBSD, can be quantitative and statistically soundly evaluated.
This could help to clearly differentiate between nano/microstructures from rolled and ECAE processed materials.
The amount of dislocation glide is much higher than that of stacking faults/twins for the rolled sample; this happens because deformation twinning is sensitive to deformation rate, and ECAE, because of geometrical reasons, proceeds much more localized and faster than rolling.

Acknowledgements
This work was supported by São Paulo State Research Foundation (FAPESP 2011/02009-0) – Brazil, ANPCyT - Argentina and the International Collaboration CONICET-DFG-Germany.

5. References

[1]. Segal V M 1995 *Mater. Sci. Eng. A* **197** 157.
[2]. Segal V M, Hartwig K T and Goforth R E 1997 *Mater. Sci. Eng. A* **224** 107.
[3]. Mishin V, Gertsman V Y, Valiev R Z and Gottstein G 1996 *Scripta Mater.* **35** 873.
[4]. Bowen J R, Gholinia A, Roberts S M and Prangnell P B 2000 *Mater. Sci. Eng. A* **28** 787.
[5]. Liu F, Zhang Y and Wang J T 2011 *Mat. Sci. Forum.* **667-669** 319.
[6]. Zhang Y, Tao N R and Lu K 2011 *Acta Materialia* **59** 6048.
[7]. Asgari S, El Danaf E, Kalidindi S R and Doherty R D 1997 *Metall. Trans A* **27** 1781.
[8]. El-Danaf E, Kaldindi S R and Doherty R D 1999 *Met. Mat. Trans. A* **30** 1223.
[9]. Ueji R, Tsuchida N, Terada D, Tsuji N, Tanaka Y, Takemura A and Kunishige K 2008 *Scripta Materialia* **59** 963.
[10]. Gutierrez-Urrutia I, Zaefferer S and Raabe D 2010 *Mater. Sci.Eng A* **527** 3552.
[11]. Wu X L and Zhu Y T 2008 *Phys Rev Lett* **101** 025503.
[12]. Han W Z, Cheng G M, Li S X, Wu S D and Zhang Z F. 2008 *Phys. Rev. Lett.* **101** 115505.
[13]. Budrovic Z, Van Swygenhoven H, Derlet P M, Van Petegem S and Schmitt B 2004 *Science* **304** 273.
[14]. Kumar K S, Suresh S, Chisholm M F, Horton J A and Wang P 2003 *Acta Mater.* **51**:387.
[15]. Shu B P, Liu L, Shen B and Hu W B 2013 *Mater. Lett.* **91** 268.
[16]. Zhao Y H, Bingert J E, Liao X Z, Cui B Z, Han K and Sergueeva A V 2006 *Adv. Mater.* **18** 2949.
[17]. Ueno H, Kakihata K, Kaneko Y, Hashimoto S and Vinogradov A 2011 *J Mater. Sci.* **46** 4276.
[18]. Ueno H, Kakihata K, Kaneko Y, Hashimoto S and Vinogradov A 2011 *Acta Mater.* **59** 7060.

[19]. Ribárik G 2008 *Modeling of diffraction patterns based on microstructural properties* Thesis (PhD in Physics) – Eötvös Loránd University, Institute of Physics, Budapest, Hungary pp. 104.
[20]. Hull D and Bacon, D J *Introduction to dislocations* 2001 Butterworth-Heinemann pp. 242.
[21]. Williamson G K and Hall W H 1953 *Acta Metallurgica* **1** 22.
[22]. Ungár T, Gubicza J, Hanák P and Alexandrov A 2001 *Mater. Sci. Eng. A* **319–321** 274.
[23]. Warren B. E. 1959 Progress in Metal Physics **8** 147.
[24]. Ungár T, Dragomir I C, Révész Á and Borbély A 1999 *J. Appl. Cryst.* **32** 992.
[25]. Schwartz, A J; Kumar, M and Adams, B L 2000 *Electron backscatter diffraction in materials science*, 2º ed**.** Klawer Academic-Plenum Publishers pp 1-20.
[26]. Nowell M M and Wright S I 2005 *Ultramicroscopy* **103** 41.
[27]. Iwahashi Y, Wang J, Horita Z, Nemoto M and Langdon T G 1996 *Scripta Mater***. 35** 143.
[28]. Kocks U F 1976 *J Eng. Mater. Technol.* **98** 76.
[29]. Mughrabi H 1988 *Rev. Phys. Appl.* **23** 367.
[30]. Pantleon W 2002 *Solid State Phenom.* **8** 773.
[31]. Estrin Y, Toth L, Brechet Y and Kim H-S. 2006 *Mater. Sci. Forum* **503** 4.